Chemical biology investigation of a triple-action, smart-decomposition antimicrobial booster based-combination therapy against “ESKAPE” pathogens

Min Wang [1], Huangsheng Pu [2,3,4], Yangfan Xu [1], Chenxuan Wu [1], Yuanxin Gu [1], Qingyun Cai [1], Guoxing Yin [5], Peng Yin [5], Chunhui Zhang [2], Wing-Leung Wong [6], Muyang Wan [2], Yugang Bai [1] and Xinxin Feng [1,7]*

[1] *State Key Laboratory of Chem-/Bio-Sensing and Chemometrics, Hunan Provincial Key Laboratory of Biomacromolecular Chemical Biology, and School of Chemistry and Chemical Engineering, Hunan University, Changsha 410082, China;*

[2] *College of Biology, Hunan University, Changsha 410082, China;*

3 *College of Advanced Interdisciplinary Studies & Hunan Provincial Key Laboratory of Novel Nano Optoelectronic Information Materials and Devices, National University of Defense Technology, Changsha 410073, China;*

[4] *Nanhu Laser Laboratory, National University of Defense Technology, Changsha 410073, China;*

[5] *Key Laboratory of Chemical Biology and Traditional Chinese Medicine Research (Ministry of Education), College of Chemistry and Chemical Engineering, Hunan Normal University, Changsha 410081, China;*

[6] *State Key Laboratory of Chemical Biology and Drug Discovery, Department of Applied Biology and Chemical Technology, The Hong Kong Polytechnic University, Hong Kong SAR 999077, China;*

[7] *Hunan Provincial Key Laboratory of Anti-Resistance Microbial Drugs, The Third Hospital of Changsha (The Affiliated Changsha Hospital of Hunan University), Changsha 410015, China*

* Corresponding author (email: xinxin_feng@hnu.edu.cn)

Abstract

The global antibiotic resistance crisis necessitates urgent solutions. One innovative approach involves potentiating antibiotics and non-antibiotic drugs with adjuvants or boosters. A major drawback of these membrane-active boosters is their limited biocompatibility, as they struggle to differentiate between prokaryotic and eukaryotic membranes. This study reports the chemical biology investigation of a dual-action oligoamidine (**OA1**) booster with a glutathione-triggered decomposition mechanism. **OA1**, when combined with other antimicrobial molecules, exhibits a triple-targeting mechanism including cell membrane disruption, DNA targeting, and intracellular enzyme inhibition. This multi-targeting mechanism not only enhances the *in vitro* and *in vivo* eradication of antibiotic-resistant "ESKAPE" pathogens, but also suppresses the development of bacterial resistance. Furthermore, **OA1** maintains its activity in bacterial cells by creating an oxidative environment, while it quickly decomposes in mammalian cells due to high glutathione levels. These mechanistic insights and design principles may provide a feasible approach to develop novel antimicrobial agents and effective anti-resistance combination therapies.

Keywords:

antimicrobial booster, oligoamidine, membrane disruption, DNA targeting, triggered degradation, anti-resistance

Introduction

Bacterial infections, especially those caused by multidrug-resistant (MDR) bacteria, pose a grave threat to public health and global healthcare economics [1,2]. The prevalence of antibiotic-resistant "ESKAPE" pathogens, consisting of two Gram-positive bacteria (*Enterococcus faecium* (*E. f*), *Staphylococcus aureus* (*S. a*)) and four Gram-negative (*Klebsiella pneumoniae* (*K. p*), *Acinetobacter baumannii* (*A. b*), *Pseudomonas aeruginosa* (*P. a*) and *Enterobacter* species), has reached an alarming level [3,4], particularly in hospital-acquired infections affecting immunocompromised or seriously ill patients [5]. With limited clinical treatment options available [2,6], there is an urgent need to address this critical challenge. Alongside developing new antibiotics with novel mechanisms [7,8], revitalizing conventional clinically used antibiotics offers a viable approach to expedite the development of effective therapeutics against drug-resistant bacteria [9–15]. Additionally, the potentiation of non-antibiotic compounds, including Food and Drug Administration (FDA)-approved drugs for non-infectious diseases and other small molecules, shows promise in the discovery of antimicrobials with innovative modes of action.

One promising strategy for antimicrobial combinations is bioavailability modulation [15], facilitated by membrane-active compounds. This approach, which has shown synergistic effects with antibiotics against MDR bacteria, involves the use of membrane-disruptive adjuvants like Colistin [16,17] and SLAP-S25 [18], as well as synthetic antimicrobial peptides and polymers [19–22]. These examples have clearly shown that, by exploiting the opportunity to develop broad-spectrum membrane-active adjuvants with high potency and multi-targeting functions, the effective suppression of resistance development is achievable. However, a crucial determinant of these membrane-active molecules lies in their limited biocompatibility, as they do not effectively distinguish prokaryotic and eukaryotic membranes. Molecular designs for membrane-disruptive adjuvants utilizing a variety of decomposition chemistry, such as guanidinium functionalized polycarbonates [23,24], selenium-containing polycaprolactones [25], imidazolium oligomers [26], and glutathione (GSH)-triggered biodegradable poly(disulfide)s [27], have been explored to address this critical issue. Nevertheless, most degradations result in a reduced cytotoxicity and antimicrobial activity simultaneously, leading to limited therapeutic improvements. Therefore, achieving selective membrane activity and discriminated degradation in bacterial and eukaryotic cells is crucial for enhancing clinical value and necessitates the additional mechanism for these membrane-active booster-based combinations.

In the present study, we report a detailed mechanistic investigation showcasing the potential to differentiate the redox homeostasis between bacteria and human host cells with a novel dual-mode antimicrobial booster **OA1** (Figure 1A). These booster-antimicrobial combinations feature collaborative membrane disruption, DNA targeting, and intracellular target inhibition, generating a broad-spectrum sensitizing activity against ESKAPE pathogens. The multitargeting primary lesion triggers the production of reactive oxygen species (ROS) in bacterial cells, resulting in a significant shift toward oxidative stress that promotes longer-lasting action of the adjuvant. In contrast, host cells experience a reductive intracellular environment that efficiently decomposes the unique disulfide linker of **OA1**, leading to a significant toxicity reduction. The selective dual-mode of action and "smart" host cell-specific degradation profile of **OA1** may address the challenge of selectivity and resistance simultaneously. Therefore, the intriguing mechanism uncovered in the present study may provide meaningful insights into the development of effective antimicrobial treatments against drug-resistant bacteria.

Experimental

Instrument information, additional synthetic procedures, and experiment protocols can be found in the Supporting Information online.

Results and discussion

Construction of a membrane-targeting antimicrobial booster model with a trigger-degradable linkage

In our previous work, we reported the synthesis of poly-cationic oligoamidines (**OA**s) with various linker units through the condensation reaction of *p*-ethylphthalimidate and different diamines (Figure 1B) [28]. These polycationic oligomers demonstrate the unique ability to selectively target bacterial membranes and DNA simultaneously [28]. Their membrane-active properties make them potential candidates for boosting antimicrobial effects, similar to other cationic membrane-active antimicrobial agents. The selectivity of these oligoamidines in disrupting bacterial cell membranes further suggests that this property may be inherited when used as boosters. To develop our model boosting agent, we incorporated a degradable linker into the oligoamidine scaffold via a polymerization process with cystamine. The resulting oligoamidine, **OA1**, contains biothiol-active degradable linkers (Figure 1B, C and Figure S1, Supporting Information online). For comparison purpose, **OA**s with inert linkers (**OA2**–**OA6**) were also synthesized. Matrix-assisted laser desorption/ionization–time-of-flight (MALDI-TOF) was employed to verify the degradability **OA1** by the detection of the oligomer in the **OA1** sample and the sub-sequent disappearance of the **OA1** signal following the treatment with GSH or dithiothreitol (DTT), as shown in Figure 1D.

An initial assessment was conducted to investigate the antibacterial efficacy of the model adjuvant. The minimum inhibitory concentration (MIC) values of the adjuvant were determined against a variety of bacteria, including the clinically isolated MDR strains. The observed MICs ranged from 0.25 to 32 μg/mL, providing compelling evidence that these polycationic oligomers possess potent antibacterial properties, effective against a broad spectrum of pathogenic microbes, irrespective of their existing antibiotic resistance (Figure 2A and Table S1, Supporting Information online). Additionally, we evaluated the MIC value against *E. coli* and the half-maximal inhibitory concentration (IC50) against RAW 264.7 cell line for a modified compound **rOA1**. The results (Figure 2B and Figure S2) revealed that the disruption of disulfide bonds in **OA1** resulted in a substantial reduction in both antibacterial activity and toxicity compared with the unmodifiable counterpart (**OA6**).

We then evaluated the ability of this model adjuvant in enhancing the antimicrobial activity of critical clinical antibiotics while also reducing antibiotic resistance in both Gram-positive and Gram-negative bacteria. For this purpose, we conducted a screening study with 32 antibiotics (Table S2), which were specifically selected by the WHO advisory group on integrated surveillance of antimicrobial resistance (AGISAR) to ensure their representativeness [29,30]. Our assessment involved an initial examination for the sy-nergistic therapeutic effects of a sub-inhibitory concentration of **OA1** in combination with these antibiotics against two laboratory strains, *S. a* and *A. b* (Tables S3 and S4), finding differential sensitization effects against various antibiotics. Checkerboard assays were next conducted to evaluation combinations with observed synergy from the above screening results. Fractional inhibitory concentration index (FICi) is calculated for each combination, and a combination is considered to be synergistic when FICi ≤ 0.5 and antagonistic when FICi > 4 [31]. Oligoamidine structures with inert linkers (**OA2**–**OA6**) were also tested for comparison. Among all the oligomers studied, **OA1** exhibited the most potent synergistic effect, sensitizing 9.4% of antibiotics against *S. a* and 25% against *A. b* (Figure 2C and Figure S3). Further analysis of the antibiotics revealed that Colistin, Kanamycin, Bacitracin, and Gentamicin displayed the best synergistic interactions with **OA1** (Figure 2D). Importantly, this positive synergy extended beyond *S. a* and *A. b*, as it also showed promising results against other clinical ESKAPE pathogens with multi-drug resistance (Figure S4). These findings unequivocally confirmed that the model adjuvant **OA1** possesses the desirable degradability and a broad-spectrum sensitizing capability.

Enhanced synergistic effects of non-antibiotic small molecules in combination with OA1

To explore new small molecule antimicrobials with **OA1** as an adjuvant, we conducted a screening process using FDA-approved non-anti-infective drugs and a library from the National Cancer Institute (NCI). The screening was performed in the presence of **OA1** at 1/4 MIC or 1/8 MIC (Figure 2E). As a result, we identified 15 promising compounds that, when combined with **OA1**, exhibited enhanced efficacy against *A. b*, bolstering their bactericidal abilities.

Among these compounds, NSC50651 emerged as the most potent hit, demonstrating a 32-fold or higher reduction in the MIC against *A. b* when used in conjunction with **OA1** at 1/8 of the MIC (Table S5). Additionally, checkerboard assays were carried out to assess the combined effects of **OA1** with fingolimod, NSC50651, NSC24113, and NSC354844. The results consistently revealed an FICi ranging from 0.09 to 0.31, indicating a synergistic interaction (Figure 2F). These findings suggest that **OA1** has the potential to significantly enhance the bactericidal properties of non-antibiotic com pounds, and the identified synergistic combinations may hold promise for combating *A. b* infections more effectively.

Collaborative membrane disruption of OA1 and cargo antimicrobial

As shown in Figure 2C, E, the interaction between **OA1** and small molecule antimicrobials, termed “cargo antimicrobial”, exhibits significant structure selectivity. Previous studies have shown that, in Gram-negative bacteria, this selectivity is partly due to the collaborative membrane lysis between the symmetric di-cationic sensitizer and the cargo antimicrobial, which plays a crucial role in the synergistic mechanism [32,33]. Building on this understanding, we hypothesize that a similar mechanism may also work in **OA1**-small molecule antimicrobial combinations and it could be effective against both Gram-positive and Gram-negative bacteria. To verify this assumption, we selected Colistin, an antibiotic that demonstrated synergistic effects with **OA1** against both *S. a* and *A. b*, to explore their synergistic antibacterial mechanism on the bacterial membrane. Firstly, the extent of membrane damage resulting from the combination of **OA1** at 8 μg/mL and Colistin at 0.5 μg/mL was examined using scanning electron microscopy (SEM). Figure 3A illustrates the presence of bacterial cell membranes with fragments and wrinkled surfaces in response to the combined treatment. It is noteworthy that these morphological alterations were not observed when either **OA1** at 8 μg/mL or Colistin at 0.5 μg/mL was used individually.

Next, we aimed to understand how **OA1**-Colistin combination interacted with the bacterial membrane. To gain insights into their potential binding targets, we examined the interaction between the **OA1**-Colistin combination and lipopolysaccharides (LPS)/phosphatidylglycerol (PG), which are major components of the outer membrane in Gram-negative bacteria and the plasma membrane in Gram-positive bacteria, respectively [34]. An LPS or lipid interference assay was utilized to assess the interaction between individual agents or their combination with exogenously added LPS or lipids. In this assay, an increase in the MIC of an agent indicates its higher affinity with the added lipid. We first studied the effect of exogenous LPS on *A. b* growth inhibition by **OA1**, Colistin, and their combination. **OA1** alone showed a 2-fold increase in MIC with LPS added (Figure 3B, C). Colistin significantly increased the ability of **OA1** binding to LPS, resulting in a 32-fold MIC change (Figure 3C). This result suggests that LPS plays a role in the activity of **OA1**-Colistin combination. We speculated a similar effect with PG, the primary phospholipid in Gram-positive bacteria (~53% of the total phospholipids in *S. a*), which was confirmed when exogenous PG diminished the synergistic effect between **OA1** and antibiotics against *S. a* (Figure 3D, E). The MIC of Colistin combined with **OA1** was also increased in the presence of exogenous PG (Figure 3E), indicating that the PG-**OA1**-Colistin interaction may drive collaborative membrane lysis in Gram-positive bacteria.

The aforementioned morphological alterations and bacterial membrane interaction observed for **OA1**-Colistin combination prompted us to further confirm the effect of combination on membrane function as a permeability barrier. This was evaluated using a standard propidium iodide (PI) assay,

where only a permeabilized bacterial membrane allows the entry of PI, leading to subsequent intercalation with DNA and a red fluorescent signal. As shown in Figure 3F and quantified in Figure 3H, these results clearly demonstrate that only the combination of **OA1** and Colistin permeabilizes the bacterial membrane, while the single drug does not show this effect. It thus is an example of synergistic interactions between agents acting on a mutual target (LPS) [15], wherein the binding of **OA1** further stabilizes the interaction between Colistin and LPS. Similar example of such mutual stabilization was reported by Song's group [28,35], in which the LPS/PG-targeting SLAP-S25 also synergized with Colistin [18]. Importantly, the permeability effect is specific to bacterial cell membranes, as the combination-treated mammalian cells displayed a minimal permeability change in the PI staining assay (Figure 3G, H). This is mainly due to the endocytosis-based model of **OA1** uptake into host cells, as previously demonstrated for other **OA**s, as well as the low affinity of Colistin for host cell membranes.

OA1 increases the accumulation of cargo antimicrobial

A direct result of the above synergistic membrane permeabilization caused by the **OA1**-Colistin combination is a significant increase in the uptake of both **OA1** and the cargo antimicrobial. To visualize this process, we examined the accumulation of a Rhodamine B-labeled Valnemulin (Val-RhB) in *E. coli*. The results showed a significant increase in intracellular Val-RhB accumulation in the presence of 32 μg/mL **OA1** (Figure 4A). Moreover, increasing the concentration of Val-RhB from 2 to 64 μg/mL further enhanced its accumulation in a dose-dependent manner (Figure 4B). This increased accumulation of Val-RhB is likely a result of the impaired bacterial membrane caused by the **OA1**-Colistin combination treatment, allowing more drugs to enter the bacterial cells. Confocal microscopy confirmed the intracellular localization of Val-RhB in the bacterial cytoplasm (Figure 4C and Figure S5). Similar results were also obtained with a fluorescent analog of Colistin (Figure S6). Moreover, the results of collaborative membrane disruption and intracellular accumulation of cargo antimicrobial were verified in *A.b* when it was treated with **OA1** and cargo antimicrobial combinations (Figure S7). These findings suggest that **OA1** disrupts the bacterial membrane, promoting the accumulation of antibiotics within bacterial cells.

Targeting of intracellular biomacromolecules by OA1-cargo antimicrobial combinations

The collaborative membrane disruption induced by the **OA1**- cargo antimicrobial combination greatly enhances the permeability of the bacterial membrane, facilitating the entry of both **OA1** and the cargo antimicrobial. Once internalized, **OA1** and the cargo antimicrobial may thus target their respective intracellular sites, including enzyme targets and DNA. To verify the interaction with these targets, we first focused on bacterial protein synthesis as a key antimicrobial mechanism of action for the cargo antimicrobial Gentamicin, selected from our previous screening. In the presence of **OA1** and Gentamicin at various combinations, fluorescence from a GFP-expressing *S. a* strain decreased approximately 1.5- to 5.1-fold compared with cells treated with either drug alone (Figure 4D). This suggests that the combination of **OA1** and Gentamicin leads to increased inhibition of bacterial protein synthesis, including GFP.

In addition to enzyme targeting, **OA1**, with its alternating amphiphilic nature, has the potential to interact with bacterial DNA that carries negative charges. Gel-retardation assays confirmed the *in vitro* interaction of **OA1** with bacterial DNA, as the mobility of the DNA was significantly inhibited in a concentration-dependent manner upon mixing with **OA1** (Figure 4E). Further investigations revealed that the antibacterial activity of **OA1** was suppressed in the presence of exogenous *E. coli* plasmid DNA in a dose-dependent manner, indicating the formation of polyplexes and deactivation of **OA1** due to its binding with DNA (Figure S8). On the other hand, Colistin, which is not targeting DNA, shows no effects on antibacterial activity under the same conditions. The intracellular interaction of **OA1** with bacterial and mammalian DNA was further investigated using confocal microscopy analysis, which showed that **OA1**-FITC (fluorescein isothiocyanate

labeled **OA1**) stained the bacterial nucleoid in *E. coli*, colocalizing with DNA staining by Hoechst 33342 (Figure 4F). However, in mammalian cells, **OA1**-FITC did not enter the nucleus despite it was able to enter the cells, as it was unlikely to be permeable to the nuclear membrane (Figure 4F). These results suggest that the off-target interaction of **OA1** with the DNA in mammalian cells is largely minimized, contributing to the low toxicity of **OA1** against mammalian cells.

Taken together, our findings strongly support the multi-mechanism of action of the **OA1**-cargo antimicrobial combination, which includes membrane targeting and subsequent collaborative membrane lysis, bacterial DNA targeting, and inhibition of intracellular enzymes. As we will discuss in the following sections, these potent primary actions may result in an increased oxidative stress in bacteria and induce the production of ROS. This oxidative cellular environment may stabilize **OA1** and is thus favorable for the long-lasting antimicrobial effect of **OA1** in bacterial cells (Figure 5A).

OA1 selectively induces ROS production in bacteria

Bacteria growing aerobically naturally generate ROS as a byproduct of their metabolic processes to enhance energy conversion from growth substrates [36]. Additionally, exposure to various lethal external stressors, including bactericidal antibiotics that inhibit he bacterial biomacromolecule synthesis, may trigger an additional cascade of ROS production via genetic pathways like toxin-antitoxin modules [37,38] (Figure 5Ai). We observed that the multi-mode **OA1**-cargo antimicrobial combination exerts significantly greater stress on bacteria, as evidenced by its faster bactericidal kinetics compared with both individual antimicrobial components and standard antibiotics (Figure 5B). To obtain more evidence, we measured ROS production in *E. coli* treated with the **OA1**-cargo antimicrobial combination at different concentrations, using a dichlorofluorescein diacetate (DCFH-DA) probe and flow cytometry (Figure S9A). We found that the ROS levels in the bacteria treated with the **OA1**-cargo antimicrobial combination were significantly higher compared with untreated bacteria, as well as to the individual antimicrobial components or standard antibiotics (Figure 5C). Conversely, since membrane permeabilization or DNA targeting by the **OA1**-cargo antimicrobial combination was absent in mammalian cells (Figures 3G and 4F), the combination exhibited only weak ROS production in mammalian cells (Figure 5D and Figure S9B). Overall, the selective accumulation of ROS in bacteria not only contributes to the enhanced antibacterial activity of the **OA1**-cargo antimicrobial combination, but also potentially preserves the **OA1** structure through the regulation of redox homeostasis (Figure 5Ai).

Modulation of cellular redox homeostasis and discriminated biodegradability of OA1 *in vivo*

The equilibrium of reducing and oxidizing reactions within live cells, known as cellular redox homeostasis, is a critical and dynamic process governing various biological responses and events [39]. Cells have evolved diverse mechanisms to regulate and manage redox balance, including antioxidant defense systems, redox-regulated transcription factors, metal ion homeostasis, and crucially, the tripeptide GSH [40]. GSH exists in both reduced (GSH) and oxidized (GSSG) forms, and the concentration of reduced GSH provides valuable insights into the cellular redox state [41]. Bacteria with overproduction of ROS as a result of stimulation by lethal external stressors, such as the **OA1**-cargo antimicrobial combination, may display a low level of GSH (Figure 5Aii). In our study, we directly measured GSH levels in bacterial and mammalian cells treated with **OA1** using a previously reported BCC probe [42]. The results revealed that the GSH level in mammalian cells was significantly higher than that in bacterial cells after the treatment (Figure 5E). This difference is likely due to the consumption of GSH by ROS in bacterial cells, leading to a discriminated biodegradability of **OA1** under cellular conditions (Figure 5Aiii).

The decomposition of **OA1** was examined indirectly through an MIC alteration assay, as previous studies have demonstrated that the decomposition product, **rOA1**, significantly loses its antimicrobial activity compared with the intact **OA1** (Figure 2B). **OA1** was incubated in both bacterial and mammalian cell cultures for 24 h to allow possible decomposition. Then, the cells were lysed to release **OA1** or its decomposed product, **rOA1**. MICs of the lysate mixture containing **OA1** or **rOA1** were assayed to determine the presence of intact **OA1** or decomposed **rOA1**. As anticipated, the antibacterial activity of **OA1** notably decreased after incubation with mammalian cells, resulting in a 16-fold increase in MIC (Figure 5F). As a control, **OA1** incubated in Dulbecco's modified Eagle medium-fetal bovine serum (DMEM-FBS) medium (used for mammalian cell growth) remained active, suggesting that **OA1** decomposition was a consequence of GSH reduction within mammalian cells. Conversely, no change in the antibacterial activity of **OA1** was observed after incubation with bacterial cells, likely due to the consumption of GSH by the overproduced ROS (Figure 5F). As an additional control, **OA6**, an oligomer with an inert linker, exhibited no significant difference in antibacterial activity following incubation with either bacterial or mammalian cells (Figure S10A). Furthermore, liquid chromatography-mass spectrometry (LC-MS) was used to directly detect the degradation product **rOA1** after treatment under different conditions (GSH *in vitro*, mammalian cells and bacterial cells), and the findings were consistent with prior observations. **rOA1** was detected in mammalian cells, consistent with treatment with GSH *in vitro*, but not in bacterial cells (Figure 5G and Figure S10B). These results indicate that **OA1** is susceptible to degradation in mammalian cells with high GSH content, while **OA6** is not. The differentiated biodegradability of **OA1** in different cellular environments underscores the importance of cellular redox homeostasis and GSH in influencing the fate of **OA1** *in vivo*, as well as in ensuring proper biocompatibility of this antimicrobial booster (Figure 5Aiv).

OA1 demonstrates a non-toxic biocompatibility profile and desirable therapeutic index

To assess the biocompatibility of polycationic oligomers, including **OA1**, we evaluated their hemolytic toxicity, cell growth inhibition, lethality to *C. elegans*, and therapeutic index in bacterial eradication (Table S6). Hemolytic toxicity was assessed using the HC50 value, representing the concentration required to lyse 50% of red blood cells (RBCs) within 1 h. Among the oligomers, **OA2** and **OA4** exhibited relatively high hemolytic toxicity with HC50 values of 44 and 79 μg/mL, respectively. However, the other oligomers displayed low hemolytic activity, with HC50 values ranging from 165 to 5000 μg/mL. For cell growth inhibition, we measured the half-maximal inhibitory concentration (IC50) against NIH/3T3 and Raw 264.7 cell lines (Table S6). **OA1** showed IC50 values ranging from 135 to 238.5 μg/mL, significantly higher than its analogues with inert linkers (<10 μg/mL). This indicates that **OA1** has superior biocompatibility compared with other cationic oligomers synthesized in this study, owing to the presence of a decomposable disulfide linker that is susceptible to reductive decomposition by GSH in mammalian cells. This biocompatibility results in the best therapeutic index among all the oligomers (Figure 5H). Together with its high LD50 (median lethal dose) against *C. elegans* (> 512 μg/mL), the favorable biocompatibility and potent antimicrobial properties of **OA1** make it a promising candidate for treating bacterial infections in animal models.

Synergy of OA1-cargo antimicrobial combination suppressed antimicrobial resistance evolution

The multi-mode of action of **OA1**-cargo antimicrobial combination is believed to contribute significantly to a resistance-suppression effect. As depicted in Figure 6A and Figure S11, bacterial strains (*B. s*, *A. b* and *E. coli*) rapidly developed resistance to individual antibiotics like Kanamycin, Ampicillin, and Gentamicin, possibly through target mutation, efflux pumps or other deactivation mechanisms [43]. In contrast, the combination of **OA1** with Gentamicin showed a remarkable

reduction in the rate of resistance generation (Figure 6A and Figure S11B). The synergistic antibacterial effect of the **OA1**-Gentamicin combination was also observed against Gentamicin-resistant *E. coli* from the resistance evolution (Figure 6B). These results clearly demonstrate the resistance-resistant nature of **OA1**-cargo antimicrobial combination. By utilizing multiple mechanisms of action from **OA1**-cargo antimicrobial combination, we may effectively combat antimicrobial resistance and slow down its development. The **OA1**-cargo antimicrobial combination shows great promise in addressing the pressing issue of antimicrobial resistance and may provide a powerful therapeutic strategy in the fight against drug-resistant bacterial infections.

Antibacterial effects of OA1-cargo antimicrobial combination in *ex vivo* and *in vivo* models

Having demonstrated attractive *in vitro* antibacterial activity in combination with various conventional antibiotics, we further investigated the antimicrobial effects of **OA1** against *ex vivo* bacterial infections in mammalian cells (Figure 6C) and *in vivo* using the *C. elegans* model. The antimicrobial activity of **OA1**, Kanamycin, and the **OA1**-Kanamycin combination was evaluated in an *A. b*-NIH/3T3 cell co-culture model (Figure 6D, E). The combination of **OA1** (at 16 or 32 μg/mL) and Kanamycin (at 2 μg/mL) significantly eradicated *A. b* from the co-cultured cells. In contrast, neither Kanamycin nor **OA1** individually exhibited significant killing effects against *A. b* in the cells. These results strongly support the bactericidal effect of **OA1**-Kanamycin combination, most likely due to their synergistic action.

To study the *in vivo* bactericidal activity of **OA1** in combination with antibiotics, *C. elegans* was used as an animal model and infected with *A. b*. When treated with a combination of 16 μg/mL **OA1** and 1 μg/mL Rifampicin, all bacteria were completely eradicated. In contrast, all single-agent treated groups showed limited efficacy (Figure 6F). Moreover, even under milder conditions using 4 μg/mL **OA1** and 0.25 μg/mL Rifampicin, the combined treatment significantly reduced bacterial loading in worms (Figure S12A). Similarly, a combination of 32 μg/mL **OA1** and 2 μg/mL Kanamycin also decreased the bacterial load with 3 log reductions in bacteria count in worms (Figure S12B). These results collectively indicate that **OA1** acts as a potential antibacterial sensitizer in an advanced infection model *in vivo*. Overall, the finding from both *ex vivo* and *in vivo* models underscores the promising therapeutic potential of the **OA1**-cargo antimicrobial combination in combating bacterial infections, opening a new approach for further research and development in this challenging area.

Conclusions

In conclusion, our study demonstrated a model biodegradable poly(disulfide) oligomer, **OA1**, which displayed significant enhancement of antibiotic potency and suppression of drug resistance against "ESKAPE" bacteria when it combined with conventional antibiotics. Additionally, **OA1** facilitated the effective repositioning of non-antibiotics for the treatment of *S. a* and *A. b* infections. **OA1**-combinations demonstrate a multiple mechanism of action, specifically involving membrane targeting and subsequent collaborative membrane lysis, bacterial DNA targeting, and inhibition of intracellular enzymes. Such strong primary lesion results in the generation of high levels of ROS, leading to an oxidative environment within bacterial cells. Notably, **OA1** could be persistent in bacterial cells while being selectively degraded within mammalian cells, offering a promising solution for improving the therapeutic index of membrane-active adjuvants. Moreover, the successful demonstration of combination therapies using **OA1** and conventional antibiotics in bacteria-mammalian cell co-culture models and an *A. b* infected *C. elegans* model further validates the potential of **OA1** as a potent adjuvant. Although **OA1** is currently a model adjuvant, further structural design, tuning, and optimization may enhance its effectiveness and biosafety in large animal models. Furthermore, the molecular design and unique mechanistic feature of **OA1** provide valuable insights for the development of new antibiotic boosters. **OA1** presents a feasibly approach to address the

biocompatibility issues commonly associated with cationic, membrane-active sensitizers. With continued research and development, such adjuvants may hold promise for advancing the field of antibiotic therapy and combating bacterial infections more effectively.

Acknowledgements This work was supported by the National Key Research and Development Program of China (2023YFD1800100 to Feng X and Bai Y), the National Natural Science Foundation of China (22177031 to Feng X, 92163127 to Bai Y, 82102415 to Wan M, and 82304277 to Zhang C), the Natural Science Foundation of Hunan Province (2024JJ4007 and 2024RC3078 to Feng X, 2022RC1107 and 2024JJ2010 to Bai Y), the Natural Science Foundation of Changsha (kq2208050 to Zhang C), the Health and Medical Research Fund (HMRF), Hong Kong SAR (22210412 to Wong WL), the Independent Research Project of the College of Advanced Interdisciplinary Studies of NUDT (22-ZZKY-03 to Pu H) and the Project of Hunan Provincial Key Laboratory of Anti-Resistance Microbial Drugs (2023TP1013). The authors sincerely thank Prof. Hang Xing (Hunan University), Dr. Kai Zhou (The First Affiliated Hospital of Southern University of Science and Technology), Dr. Hui Wang (Peking University People's Hospital), and Dr. Cuiyan Tan (Fifth Affiliated Hospital of Sun Yat-sen University) for providing bacterial strains. Also thank Dr. Haijun Tu (Hunan University) for kindly providing the C. elegans strain. And thank Dr. Ran Xie (Nanjing University) for kindly providing the Dansyl-PMBN. The authors thank the Analytical Instrumentation Center of Hunan University for the assistance with instrumental analysis.

Conflict of interest The authors declare the following competing financial interest(s): Yugang Bai and Xinxin Feng are inventors on a patent (ZL 2022 10121259.7) for the oligomer reported in this manuscript. The authors declare no competing financial interests.

References

1. Adeyi OO, Baris E, Jonas OB, Irwin A, Berthe FCJ, Le Gall FG, Marquez PV, Nikolic IA, Plante CA, Schneidman M. Drug-resistant infections: A threat to our economic future. 2017. http://documents. worldbank.org/curated/en/323311493396993758/final-report

2. Group IC. No time to wait: Securing the future from drug-resistant infections. 2019. https://www.who.int/publications/i/item/no-time-to-wait-securing-the-future-from-drug-resistant-infections

3. De Oliveira DMP, Forde BM, Kidd TJ, Harris PNA, Schembri MA, Beatson SA, Paterson DL, Walker MJ. *Clin Microbiol Rev*, 2020, 33: e00181-19

4. Tacconelli E, Carrara E, Savoldi A, Harbarth S, Mendelson M, Monnet DL, Pulcini C, Kahlmeter G, Kluytmans J, Carmeli Y, Ouellette M, Outterson K, Patel J, Cavaleri M, Cox EM, Houchens CR, Grayson ML, Hansen P, Singh N, Theuretzbacher U, Magrini N, Aboderin AO, Al-Abri SS, Awang Jalil N, Benzonana N, Bhattacharya S, Brink AJ, Burkert FR, Cars O, Cornaglia G, Dyar OJ, Friedrich AW, Gales AC, Gandra S, Giske CG, Goff DA, Goossens H, Gottlieb T, Guzman Blanco M, Hryniewicz W, Kattula D, Jinks T, Kanj SS, Kerr L, Kieny MP, Kim YS, Kozlov RS, Labarca J, Laxminarayan R, Leder K, Leibovici L, Levy-Hara G, Littman J, Malhotra-Kumar S, Manchanda V, Moja L, Ndoye B, Pan A, Paterson DL, Paul M, Qiu H, Ramon-Pardo P, Rodríguez-Baño J, Sanguinetti M, Sengupta S, Sharland M, Si-Mehand M, Silver LL, Song W, Steinbakk M, Thomsen J, Thwaites GE, van der Meer JW, Van Kinh N, Vega S, Villegas MV, Wechsler-Fördös A, Wertheim HFL, Wesangula E, Woodford N, Yilmaz FO, Zorzet A. *Lancet Infect Dis*, 2018, 18: 318– 327

5. Peleg AY, Hooper DC. *N Engl J Med*, 2010, 362: 1804–1813

6. Laxminarayan R, Duse A, Wattal C, Zaidi AKM, Wertheim HFL, Sumpradit N, Vlieghe E, Hara GL, Gould IM, Goossens H, Greko C, So AD, Bigdeli M, Tomson G, Woodhouse W, Ombaka E, Peralta AQ, Qamar FN, Mir F, Kariuki S, Bhutta ZA, Coates A, Bergstrom R, Wright GD, Brown ED, Cars O. *Lancet Infect Dis*, 2013, 13: 1057– 1098

7. Silver LL. *Clin Microbiol Rev*, 2011, 24: 71–109

8. Lakemeyer M, Zhao W, Mandl FA, Hammann P, Sieber SA. *Angew Chem Int Ed*, 2018, 57: 14440–14475

9. Brown D. *Nat Rev Drug Discov*, 2015, 14: 821–832

10. Zheng W, Sun W, Simeonov A. *Br J Pharmacol*, 2018, 175: 181–191

11. Tyers M, Wright GD. *Nat Rev Microbiol*, 2019, 17: 141–155

12. Zhu M, Tse MW, Weller J, Chen J, Blainey PC. *Ann New York Acad Sci*, 2021, 1496: 82–96

13. Ejim L, Farha MA, Falconer SB, Wildenhain J, Coombes BK, Tyers M, Brown ED, Wright GD. *Nat Chem Biol*, 2011, 7: 348–350

14. Douafer H, Andrieu V, Phanstiel Iv O, Brunel JM. *J Med Chem*, 2019, 62: 8665–8681

15. Sullivan GJ, Delgado NN, Maharjan R, Cain AK. *Curr Opin Microbiol*, 2020, 57: 31–40

16. MacNair CR, Stokes JM, Carfrae LA, Fiebig-Comyn AA, Coombes BK, Mulvey MR, Brown ED. *Nat Commun*, 2018, 9: 458

17. French S, Farha M, Ellis MJ, Sameer Z, Côté JP, Cotroneo N, Lister T, Rubio A, Brown ED. *ACS Infect Dis*, 2020, 6: 1405–1412

18. Song M, Liu Y, Huang X, Ding S, Wang Y, Shen J, Zhu K. *Nat Microbiol*, 2020, 5: 1040–1050

19. Namivandi-Zangeneh R, Sadrearhami Z, Dutta D, Willcox M, Wong EHH, Boyer C. *ACS Infect Dis*, 2019, 5: 1357–1365

20. Ding X, Yang C, Moreira W, Yuan P, Periaswamy B, de Sessions PF, Zhao H, Tan J, Lee A, Ong KX, Park N, Liang ZC, Hedrick JL, Yang YY. *Adv Sci*, 2020, 7: 2001374

21. Si Z, Lim HW, Tay MYF, Du Y, Ruan L, Qiu H, Zamudio-Vazquez R, Reghu S, Chen Y, Tiong WS, Marimuthu K, De PP, Ng OT, Zhu Y, Gan Y-, Chi YR, Duan H, Bazan GC, Greenberg EP, Chan-Park MB, Pethe K. *Angew Chem Int Ed*, 2020, 59: 6819–6826

22. Xiong M, Lee MW, Mansbach RA, Song Z, Bao Y, Peek Richard M. J, Yao C, Chen LF, Ferguson AL, Wong GCL, Cheng J. *Proc Natl Acad Sci USA*, 2015, 112: 13155–13160

23. Chin W, Zhong G, Pu Q, Yang C, Lou W, De Sessions PF, Periaswamy B, Lee A, Liang ZC, Ding X, Gao S, Chu CW, Bianco S, Bao C, Tong YW, Fan W, Wu M, Hedrick JL, Yang YY. *Nat Commun*, 2018, 9: 917

24. Yang C, Lou W, Zhong G, Lee A, Leong J, Chin W, Ding B, Bao C, Tan JPK, Pu Q, Gao S, Xu L, Hsu LY, Wu M, Hedrick JL, Fan W, Yang YY. *Acta BioMater*, 2019, 94: 268–280

25. Li Y, Ma X, Zhang J, Pan X, Li N, Chen G, Zhu J. *ACS Macro Lett*, 2022, 11: 1349–1354

26. Yuan Y, Lim DSW, Wu H, Lu H, Zheng Y, Wan ACA, Ying JY, Zhang Y. *BioMater Sci*, 2019, 7: 2317–2325

27. Guo J, Zhang S, Tao Y, Fan B, Tang W. *Polym Chem*, 2022, 13: 6637– 6649

28. Bai S, Wang J, Yang K, Zhou C, Xu Y, Song J, Gu Y, Chen Z, Wang M, Shoen C, Andrade B, Cynamon M, Zhou K, Wang H, Cai Q, Oldfield E, Zimmerman SC, Bai Y, Feng X. *Sci Adv*, 2021, 7: eabc9917

29. World Health Organization. Critically important antimicrobials for human medicine. Bogota: World Health Organization, 2019. https:// www.who.int/publications/i/item/9789241515528

30. World Health Organization. World health organization model list of essential medicines: 22nd list (2021). 2021. https://www.who.int/ publications/i/item/WHO-MHP-HPS-EML-2021.02

31. Odds FC. *J AntiMicrob ChemoTher*, 2003, 52: 1

32. Zhou Y, Huang W, Lei E, Yang A, Li Y, Wen K, Wang M, Li L, Chen Z, Zhou C, Bai S, Han J, Song W, Ren X, Zeng X, Pu H, Wan M, Feng X. *ACS Chem Biol*, 2022, 17: 3178–3190

33. Lei E, Tao H, Jiao S, Yang A, Zhou Y, Wang M, Wen K, Wang Y, Chen Z, Chen X, Song J, Zhou C, Huang W, Xu L, Guan D, Tan C, Liu H, Cai Q, Zhou K, Modica J, Huang SY, Huang W, Feng X. *J Am Chem Soc*, 2022, 144: 10622–10639

34. Ciumac D, Gong H, Hu X, Lu JR. *J Colloid Interface Sci*, 2019, 537: 163–185

35. Wang J, Song J, Chen X, Guo RT, Wang Y, Huang G, Zheng N, Hu P, Feng X, Bai Y. *CCS Chem*, 2022, 4: 3573–3586

36. Brynildsen MP, Winkler JA, Spina CS, MacDonald IC, Collins JJ. *Nat Biotechnol*, 2013, 31: 160–165

37. Kohanski MA, Dwyer DJ, Hayete B, Lawrence CA, Collins JJ. *Cell*, 2007, 130: 797–810

38. Van Acker H, Coenye T. *Trends Microbiol*, 2017, 25: 456–466

39. Le Gal K, Schmidt EE, Sayin VI. *Antioxidants*, 2021, 10: 1377

40. Espinosa-Diez C, Miguel V, Mennerich D, Kietzmann T, Sánchez- Pérez P, Cadenas S, Lamas S. *Redox Biol*, 2015, 6: 183–197

41. Monostori P, Wittmann G, Karg E, Túri S. *J Chromatography B*, 2009, 877: 3331–3346

42. Yin GX, Niu TT, Gan YB, Yu T, Yin P, Chen HM, Zhang YY, Li HT, Yao SZ. *Angew Chem Int Ed*, 2018, 57: 4991–4994

43. Darby EM, Trampari E, Siasat P, Gaya MS, Alav I, Webber MA, Blair JMA. *Nat Rev Microbiol*, 2023, 21: 280–295

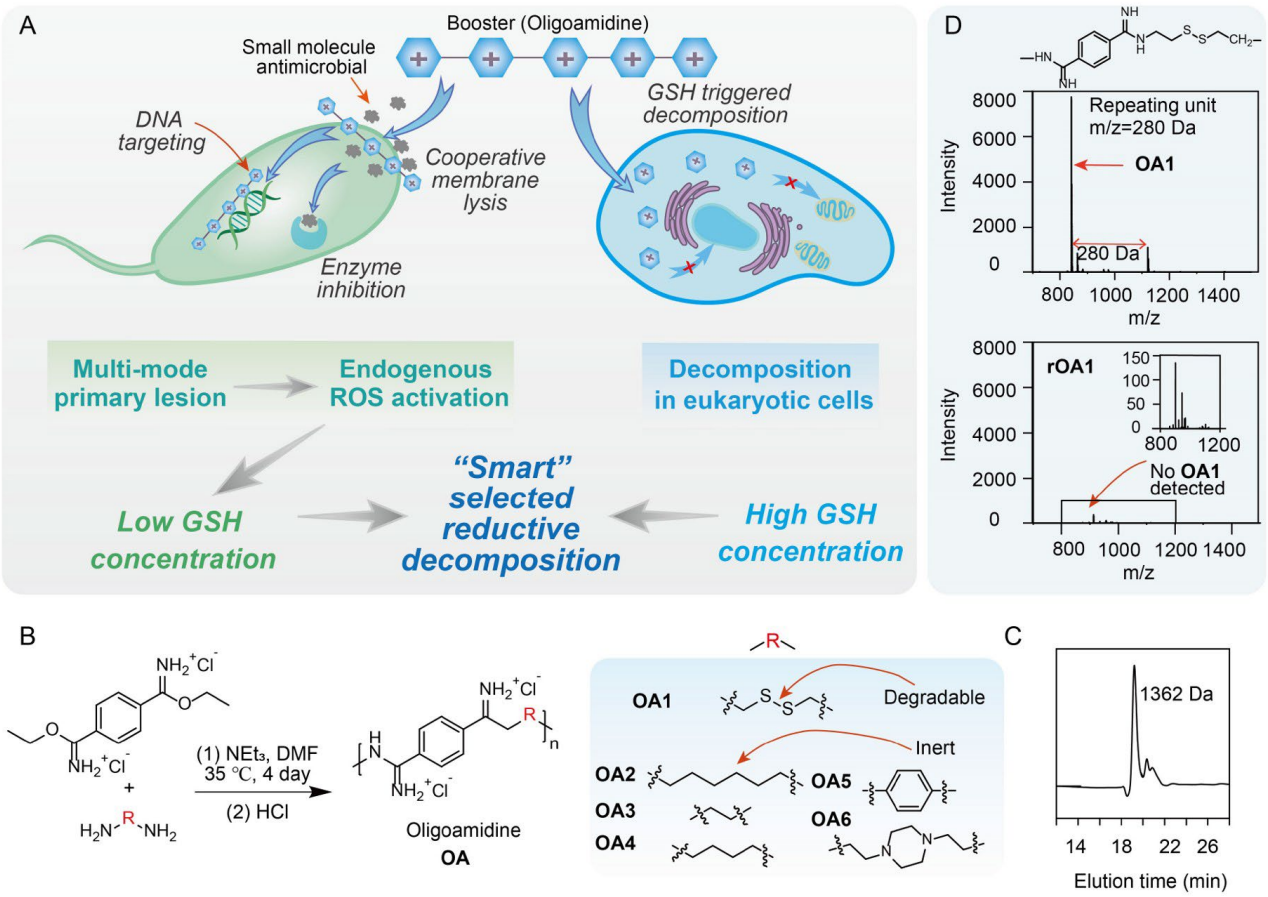

Figure 1. Design and characterization of **OA**. (A) Scheme for an antimicrobial booster (oligoamidine) with a multi-mode mechanism including collaborative membrane disruption, DNA targeting, and intracellular enzyme inhibition. (B) Synthesis of a series of oligoamidines. (C) Gel permeation chromatogram of **OA1** with marked molecular weight in Dalton (Da). (D) MALDI-TOF spectrum of **OA1** and **rOA1** (the decomposed product of **OA1**); *m*/*z*, mass/charge ratio.

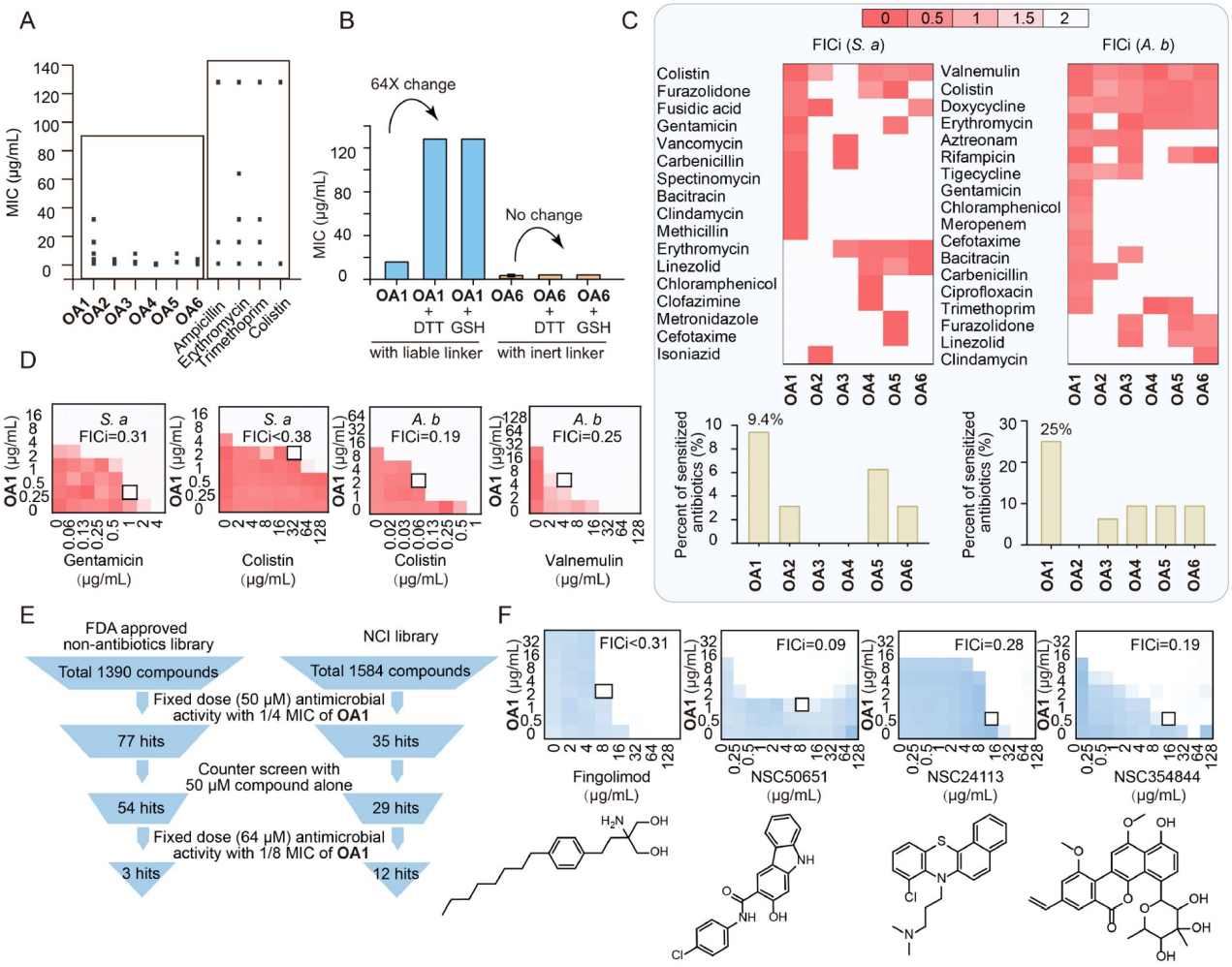

Figure 2. Antimicrobial activity of **OA**-antibiotic combinations against *S. a* and *A. b*. (A) MIC values of the antimicrobial oligoamidine and conventional antibiotics against "ESKAPE" strains. (B) The MIC values of **OA1** and **OA6** against *E. coli* after degradation by GSH or DTT. (C) Heat map of FICi values for different **OA**-antibiotic combinations against *S. a* and *A. b*. The darker color represents a better synergy effect. (D) Checkerboard assays of antibiotic in combination with **OA1** against *S. a* and *A. b*. (E) A screening of FDA-approved non-antibiotics and NCI library resulted in either 3 hits or 12 hits in combination with **OA1** against *A. b*. (F) Checkerboard assays of hit from both the FDA and NCI library in combination with **OA1** against *A. b*.

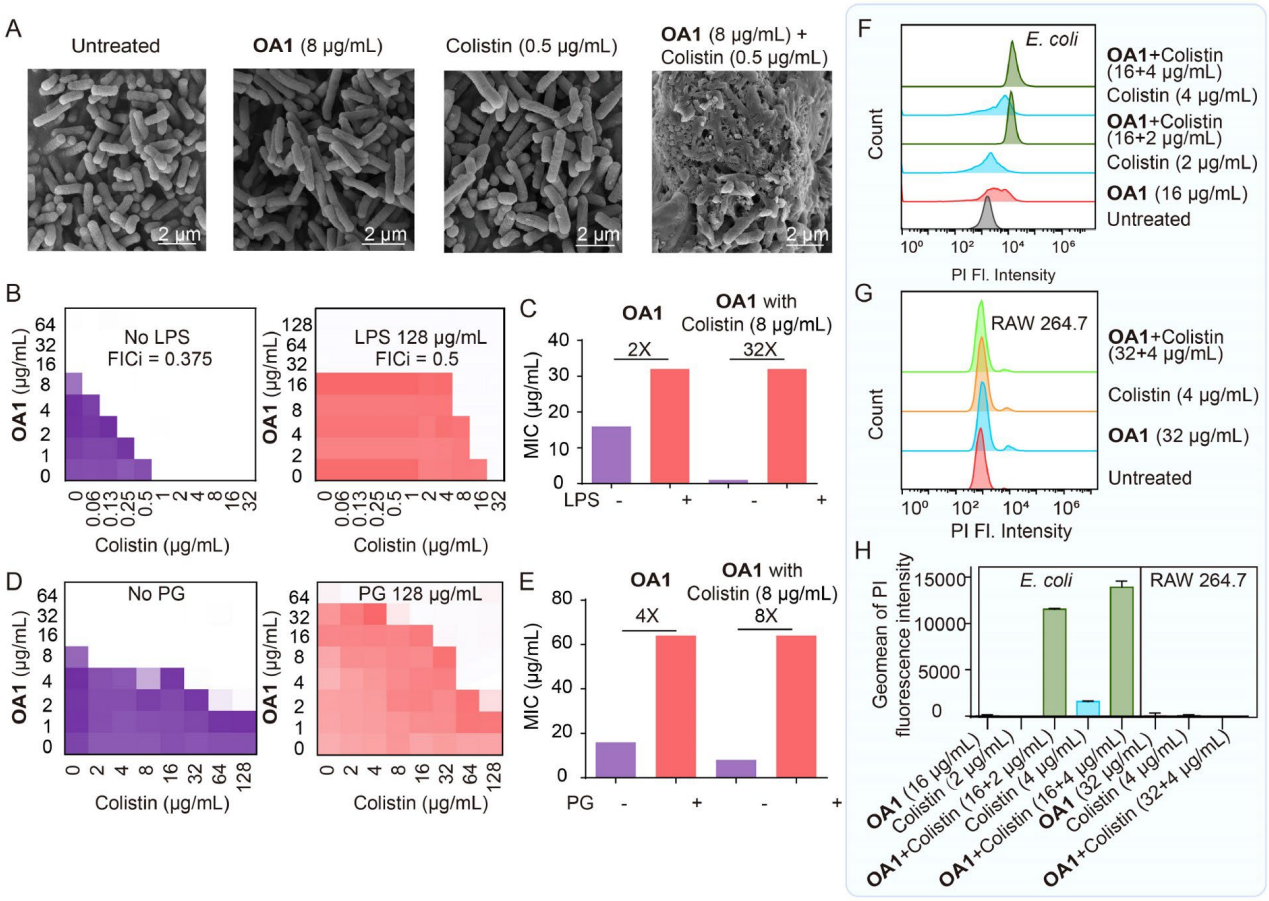

Figure 3. Investigation of the cooperative membrane damage mechanism. (A) SEM images of **OA1**-treated, Colistin-treated and combinations-treated *E. coli*, with untreated sample serving as controls. (B) Checkerboard assay results of **OA1**-Colistin agaisnt *A. b* in the absence (left panel) and presence (right panel) of 128 μg/mL LPS. (C) Quantitative analysis of LPS interference on MICs of **OA1** and the combination (**OA1** in combination with 8 μg/mL Colistin). (D) Checkerboard assay results of **OA1**-Colistin agaisnt *S. a* in the absence (left panel) and presence (right panel) of 128 μg/mL PG. (E) Quantitative analysis of PG interference on MICs of **OA1** and the combinations (**OA1** in combination with 8 μg/mL Colistin). (F, G) Flow cytometry results of PI assay, indicating the membrane permeability of bacteria and RAW 264.7 cells after treatment with **OA1**, Colistin, or their combination. (H) Quantification of the membrane permeability in bacteria and RAW 264.7 cells treated with different agents by calculating the geometric mean of PI fluorescence over respective cell volume. Data shown in (H) are presented as the mean ± s.d. of at least two independent experiments.

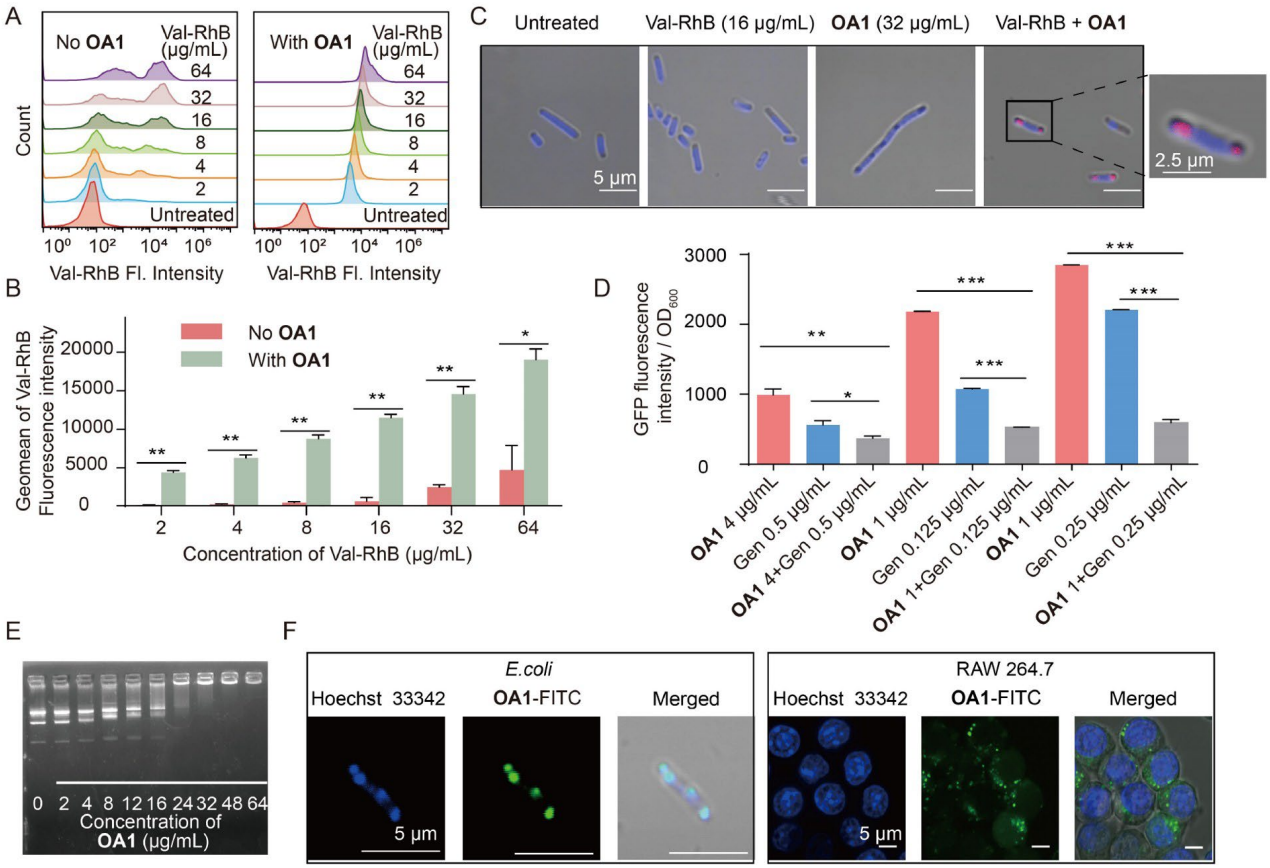

Figure 4. **OA1** promotes the accumulation of antibiotics in bacteria and targets intracellular biomacromolecules. (A) The intracellular accumulation of Val-RhB in the absence or presence of **OA1**. (B) Quantification of the intracellular accumulation in *E. coli* treated with different agents by calculating the geometric mean of Val-RhB fluorescence over respective cell volume. (C) Confocal images of *E. coli* treated by Val-RhB in the absence or presence of **OA1**. (D) Effects of **OA1**, Gentamicin (Gen) or their combinations on GFP expression in *S. a*. (E) Gel retardation assay results of DNA (40 μg/mL) mixed with **OA1** at different concentrations. (F) Confocal images of *E. coli* and RAW 264.7 cells stained by **OA1**-FITC at 32 μg/mL (green) and Hoechst (blue). Statistical significances were analyzed using student's *t*-test and significant differences between groups are marked with an asterisk. *, ** and *** indicate $P \leq 0.05$, $P \leq 0.01$, and $P \leq 0.001$, respectively. Data shown in (B) and (D) are presented as the mean ± s.d. of at least two independent experiments.

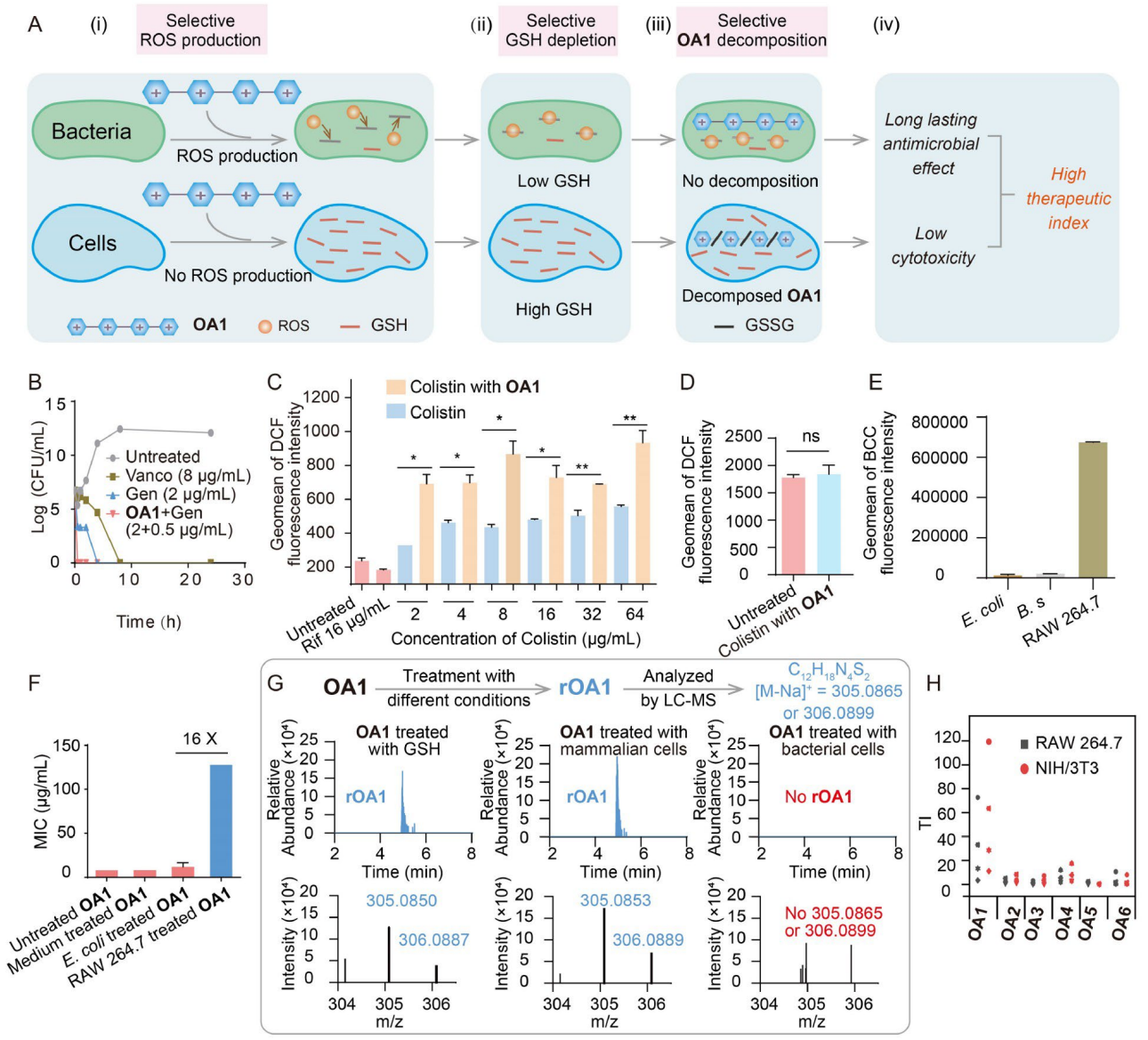

Figure 5. **OA1** selectively induces ROS production in bacteria and exhibits differential biodegradability *in vivo*. (A) A scheme of selective induction of ROS production in bacteria by **OA1**. (B) Killing kinetics of *S. a* in the presence of Vancomycin (Vanco), Gentamicin (Gen), and **OA1**-Gentamycin combinations (**OA1**+Gen). (C) ROS generation by Rifampicin (Rif), Colistin and **OA1** (32 μg/mL) and Colistin combination in *E. coli* at different concentrations as probed by DCFH-DA. (D) ROS generation by **OA1**-Colistin (32+32 μg/mL) combination in RAW 264.7 as probed by DCFH-DA. (E) GSH content in *E. coli*, *B. s* and RAW 264.7 cells after treatment with **OA1** (32 μg/mL) as probed by BCC. (F) *S. a* MIC values of **OA1** or its decomposition product treated with *E. coli* or RAW 264.7 cells. (G) **OA1** (128 μg/mL) decomposed in mammalian cells but not decomposed in bacteria cells. (H) Therapeutic indices of the antimicrobial oligoamidine in RAW 264.7 and NIH/3T3 cells. Statistical significances were analyzed using student's *t*-test and significant differences between groups are marked with an asterisk. *, ** and *** indicate $P \leq 0.05$, $P \leq 0.01$, and $P \leq 0.001$, respectively. Data shown in (C–F) are presented as the mean ± s.d. of at least two independent experiments.

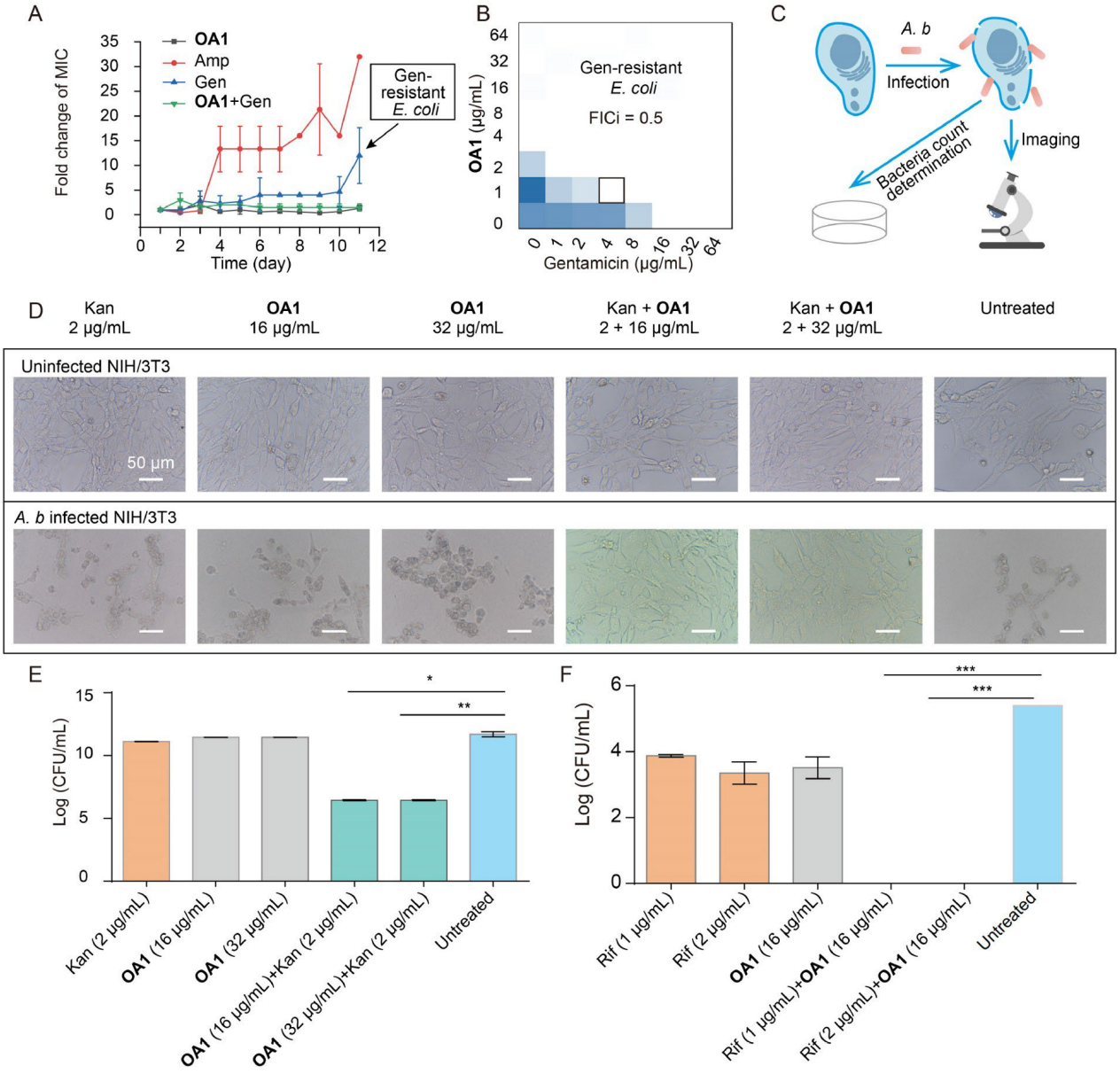

Figure 6. **OA1** rescues the activity of conventional antibiotics in bacteria-infected eukaryotic cell and *C. elegans* models. (A) Resistance generation rate of **OA1** and Ampcillin (Amp), Gentamicin (Gen) and **OA1**-Gentamycin combination (**OA1**+Gen) against *E. coli*. (B) Checkerboard assays of **OA1** and Gentamicin on Gentamicin-resistant *E. coli* obtained from (A). (C) A scheme of bacteria-infected eukaryotic cells (NIH/3T3) model. (D and E) Rescue of *A. b*-infected eukaryotic cells (NIH/3T3) with **OA1**, Kanamycin (Kan) and their combinations. (F) Rescue of *A. b*-infected *C. elegans* with **OA1**, Rifampicin (Rif) and their combinations. Statistical significances were analyzed using student's *t*-test and significant differences between groups are marked with an asterisk. *, ** and *** indicate $P \leq 0.05$, $P \leq 0.01$, and $P \leq 0.001$, respectively. Data shown in (A, E, and F) are presented as the mean ± s.d. of at least 2 independent experiments.